PLOS COMPUTATIONAL BIOLOGY

RESEARCH ARTICLE

Physics-based tissue simulator to model multicellular systems: A study of liver regeneration and hepatocellular carcinoma recurrence

Luciana Melina Luque[1]*, **Carlos Manuel Carlevaro**[1,2]*, **Camilo Julio Llamoza Torres**[3], **Enrique Lomba**[4]

1 Instituto de Física de Líquidos y Sistemas Biológicos - CONICET. La Plata, Argentina, **2** Departamento de Ingeniería Mecánica, Universidad Tecnológica Nacional, Facultad Regional La Plata, La Plata, Argentina, **3** Hospital Clínico Universitario Virgen de la Arrixaca. Murcia, España, **4** Instituto de Química Física Rocasolano - CSIC. Madrid, España

* lluque@iflysib.unlp.edu.ar (LML); manuel@iflysib.unlp.edu.ar (CMC)

OPEN ACCESS

Citation: Luque LM, Carlevaro CM, Llamoza Torres CJ, Lomba E (2023) Physics-based tissue simulator to model multicellular systems: A study of liver regeneration and hepatocellular carcinoma recurrence. PLoS Comput Biol 19(3): e1010920. https://doi.org/10.1371/journal.pcbi.1010920

Editor: Roeland M.H. Merks, Leiden University Faculty of Science: Universiteit Leiden Faculteit der Wiskunde en Natuurwetenschappen, NETHERLANDS

Received: March 1, 2022

Accepted: February 3, 2023

Published: March 6, 2023

Data Availability Statement: All relevant data are within the manuscript and its Supporting information files. The code used for running experiments is available at https://github.com/lmluque/abm.

Funding: This work was supported by the European Union Horizon 2020 Research and Innovation Staff Exchange programme under the Marie Sklodowska-Curie grant agreement No.

Abstract

We present a multiagent-based model that captures the interactions between different types of cells with their microenvironment, and enables the analysis of the emergent global behavior during tissue regeneration and tumor development. Using this model, we are able to reproduce the temporal dynamics of regular healthy cells and cancer cells, as well as the evolution of their three-dimensional spatial distributions. By tuning the system with the characteristics of the individual patients, our model reproduces a variety of spatial patterns of tissue regeneration and tumor growth, resembling those found in clinical imaging or biopsies. In order to calibrate and validate our model we study the process of liver regeneration after surgical hepatectomy in different degrees. In the clinical context, our model is able to predict the recurrence of a hepatocellular carcinoma after a 70% partial hepatectomy. The outcomes of our simulations are in agreement with experimental and clinical observations. By fitting the model parameters to specific patient factors, it might well become a useful platform for hypotheses testing in treatments protocols.

Author summary

We introduce an off-lattice agent-based model to simulate tissue-scale features that emerge from basic biological and biophysical cell processes. In order to calibrate and validate our model, we have considered the liver regeneration response after a 30% partial hepatectomy in which the liver recovers its original volume due to the hypertrophy of the hepatocytes. Subsequently, we have modeled the same process but after a 70% partial hepatectomy, in which the liver recovers its original volume due to the hypertrophy and the proliferation of the hepatocytes. Unfortunately, the precise mechanisms of initiating, promoting and terminating regenerative responses remain unknown. As a consequence, we have proposed a modeling approach in which such processes are regulated by a

734276, which funded both the stays of E.L. at UNLP and C.M.C. and L.M.L. at IQFR-CSIC. L.M.L. is supported by CONICET postdoctoral fellowship (RESOL-2020-134-APN-DIR#CONICET). E.L. also acknowledges funding from the Agencia Estatal de Investigación under grant no. PID2020-115722GB-C22. The funders had no role in study design, data collection and analysis, decision to publish, or preparation of the manuscript.

Competing interests: The authors have declared that no competing interests exist.

hypothetical substrate that diffuses in the cell microenvironment. As a further test, we have, in one hand, implemented our model to predict the liver response after a 50% partial hepatectomy and, on the other hand, explored our model's ability to account for the recurrence of a hepatocellular carcinoma. The outcomes of our simulations agree with experimental data and clinical observations, which comes to underline the significant descriptive and predictive power of this computational approach. Even though our model needs to be further extended to incorporate patient specific clinical data, these results are a promising step in the direction of a personalized estimation of tissue dynamics from a limited number of measurements carried out at diagnosis.

1 Introduction

Many significant multicellular system problems such as tissue engineering, evolution in bacterial colonies, and tumor metastasis can only be understood by studying how individual cells grow, divide, die, move, and interact. Tissue-scale dynamics emerges as cells are influenced by biochemical and biophysical signals in their microenvironment, bearing in mind that cells themselves continually remodel their own microenvironment. Thus, the ideal scenario to study a multicellular system's biology must simultaneously address: tissue microenvironments with multiple diffusing chemical signals (e.g., oxygen, drugs, and signalling factors), and the dynamics of many mechanically and biochemically interacting cells.

To that aim, mechanistic dynamical systems models described by ordinary differential equations have been developed [1–10] (cf. those reviewed in [11] and [12]). Even though these models are very useful, they lack the spatial resolution that would enable the examination of intratumoral heterogeneity and its correlation with treatment efficacy. This is a relevant feature since intratumoral heterogeneity has become a central element for understanding important aspects of cancer treatment such as drug resistance and biomarkers [13, 14].

A widely used modeling paradigm in the study of complex biological systems is the *agent-based model* (ABM) [15, 16]. ABMs are implemented mainly to simulate the actions, behaviors and interactions of autonomous individual or collective entities, with the aim of exploring the impact of an agent or a type of behavior in the system. Agents are independent units trying to accomplish a set of goals. The purpose of an ABM is to explore variations in the system behavior due to agent characteristics or rules. These attempt to emulate the general behavior of the system and predict the patterns of complex phenomena. Agents behave independently, but they react to the environment, modify system properties, and incorporate new agents. They also have the ability to "learn", that is, to avoid previously unsuccessful decisions and favor successful ones, as well as to "adapt", i.e. change their behavior in response to variations of the properties of the system. Their basic advantage is that they provide predictive power on a large scale [17].

In many cases the system being modelled is usually comprised of millions of components. In those cases a great level of abstraction/simplification must be applied to the model to render it useful [18] (we refer the reader to [19] for as extensive discussion on the accuracy of computational models). For that reason, once a preliminary model has been constructed it must be subjected to verification, calibration and validation. Verification is the process of determining how accurately prior knowledge and underlying assumptions have been translated into mathematical form. Calibration is the process by which parameters in a model are adjusted so as to match model performance to experimental data. Finally, model validation is the process of

evaluating model performance against the primary design goal. In the case of biological models, this usually aims at achieving a close match between model and experiment [20].

In a medical context, ABMs should allow simulating clinical trials in sufficient detail to study the subject's response to changes in therapy in simulations, rather than in patients. ABM have been used to study many different aspects of cancer, including tumor growth, cancer cell migration, metabolism, evolutionary dynamics, metastasis, angiogenesis and the role of cancer stem cells [21–34]. The reader is referred the extensive review by Norton and coworkers [35] for a more detailed presentation of the potential of ABMs in the context of cancer modeling.

Here, we will present a mechanistic off-lattice agent-based model to simulate tissue-scale features that emerge from basic biological and biophysical cell processes. This ABM will be validated and put to test for modeling the unusual ability of the liver to regenerate [36]. Even when 70% of its mass is surgically removed, the remnant portion expands to compensate for the lost tissue and functions [37]. The multilobular structure of the liver allows the surgical resection of a lobe of choice to achieve different degrees by partial hepatectomy (PH). Because the resection of lobes does not induce damage to the remaining tissue, PH is a clean model. Therefore, liver regeneration after PH has long been an excellent experimental model for tissue regeneration. Furthermore, although the liver consists of various types of cells, hepatocytes account for about 80% of liver weight and about 70% of all liver cells [38]. Thus, hepatocytes provide an ideal starting point to study the relation of organ size with number and size of cells.

It has been generally accepted that liver regeneration depends mainly on the proliferation of hepatocytes [37, 39, 40]. However, there are several reports showing hypertrophy of hepatocytes in the regenerated liver [41–43]. Miyaoka et al. [44, 45] performed a series of experiments and found that although a number of studies indicated that almost all hepatocytes proliferate after 70% PH, cellular hypertrophy significantly contributes to liver regeneration as well. They showed that hepatocytes undergo cell division only about 0.7 times on average in the regeneration from 70% PH, and that at early stages, the regeneration totally depends on the hypertrophy of hepatocytes. In contrast, liver regeneration after 30% PH is solely due to hypertrophy.

Therefore, liver regeneration process is a perfect scenario to test and calibrate our model. On the other hand, post-hepatectomy liver failure is a serious complication after liver resection and its incidence varies from 1.2 to 32% [46–49]. It is defined as functional deterioration of the liver associated with an increased international normalized ratio (INR)—a measurement of how long it takes blood to form a clot-, and hyperbilirubinemia typically starting after the fifth postoperative day [46]. There are recommendations that post-hepatectomy liver failure could be prevented if the remnant liver size is above 20% of its original size in patients with normal liver function, and 30 – 40% in patients with steatohepatitis or cirrhosis [50, 51]. Nevertheless, even with adequate preoperative assessments, post-hepatectomy liver failure is a major contributor to mortality rates of up to 5% after liver resection [52, 53]. Various patient-related factors (age, comorbidities such previous chemotherapy, cirrhosis, fibrosis, cholestasis, and steatosis), and surgery-related factors (extent of resection, blood loss, and ischemia reperfusion injury) affect the regenerative capacity of the remnant liver [54, 55]. Given all these numerous factors, estimating the adequate extent of the hepatectomy, and individual regenerative capacity, remain significant challenges for clinicians and scientists. It is to be stressed here that the regeneration process is controlled by different transcriptomic signatures depending on the intensity, duration and etiology of liver injury [56]. Consequently, different transcripts can modulate the results of the regeneration processes.

In any case, according to the Barcelona Clinic Liver Cancer (BCLC) staging system [57], hepatic resection (partial hepatectomy) can be considered as a curative treatment for patients with stage 0-A uninodular hepatocellular carcinoma (HCC) who maintain preserved liver function and without portal hypertension. The prognosis of HCC patients has improved

because of advances in radiologic assessment, patient selection, operative techniques, and perioperative care [58, 59]. On the other hand, long-term prognosis of patients with HCC after liver resection is often affected by high tumor recurrence rates that reach 40 – 70% within 5 years [60]. This is an issue that must urgently be addressed, and where we believe that a well calibrated computational model that succeeds on modeling the liver regeneration processes and HCC evolution, would complement the clinical trials, once fed-in with specific patient data. Moreover, liver regeneration is the basic element for the maintenance of liver function and size during homeostasis and liver injury (acute and chronic). Understanding the mechanisms of hepatic regeneration, from its cellular origins and signaling mechanisms, is essential to design specific regeneration models. Making these models available in a more "accessible" way that allows for a quicker evaluation of the influence of certain factors on regeneration processes, unlike the "classical" models, would then facilitate the optimization the different diagnostic strategies (time intervals for hepatocarcinoma screening) and treatments (recurrence rate compared to ablative therapies, immunotherapy, response to sequential therapies). The approach here presented might well constitute a potential tool to evaluate biomarkers, such as circulating tumor cells (determined by liquid biopsy) and their correlation with the rate of tumor growth.

The manuscript is organized as follows: After a brief description of the biological model, our agent-based model and the tumor growth model in section 2, we calibrate and validate our model against literature data [44, 45, 61–64], for two cases of liver regeneration: 30% PH and 70% PH (Sections 3.1.1 and 3.1.2 respectively). Then we test our model for a 50% PH in section 3.1.3. Finally, we have simulated the recurrence of a hepatocellular carcinoma after a PH and present our most significant results in section 3.2. Therein, all our results are commented and analyzed in the light of experimental (data obtained on mice) and clinical data. Discussion and future prospects are presented in section 4.

2 Materials and methods

2.1 Biological model

The liver is a highly complex organ, which removes drugs and toxins from the blood. It is characterized by its multi-scale architecture (Fig 1) which consists of four lobes: the right lobe, the left lobe, the caudate lobe, and the quadrate lobe, which are further divided into eight segments based in the Couinaud system, also known as hepatic segments [65]. Each segment has its own vascular inflow, outflow and biliary drainage. The division of the liver into independent units means that segments can be resected without damaging the remaining segments. Hepatic parenchyma is organized in repetitive functional units called liver lobules. The lobules are roughly hexagonal prisms, and consist of plates of hepatocytes, and sinusoids radiating from a central vein towards an imaginary perimeter of interlobular portal triads. The portal triad is a distinctive component of a lobule, which can be found running along each of the lobule's corners. It consists of the hepatic artery, the portal vein and the common bile duct. The central vein joins the hepatic artery and the portal vein to carry blood out from the liver [66]. A recent work reported that this particular structures remain during the liver regeneration process [67]. Even though hepatocytes (liver parenchymal cells) account for about 80% of liver weight and about 70% of all liver cells, the liver also has other type of cells named nonparenchymal cells: endothelial cells, Kupffer cells (macrophages resident in the liver), and biliary-duct cells [38].

One of the main characteristics of the liver is its high regenerative capacity after injury. Even when 70% of its mass is surgically removed, the remnant portion expands to compensate for the lost tissue and functions [37, 68]. Liver resection is the most common liver surgery and consists of removal of liver tissue due to focal lesions, most often malignant tumors and living

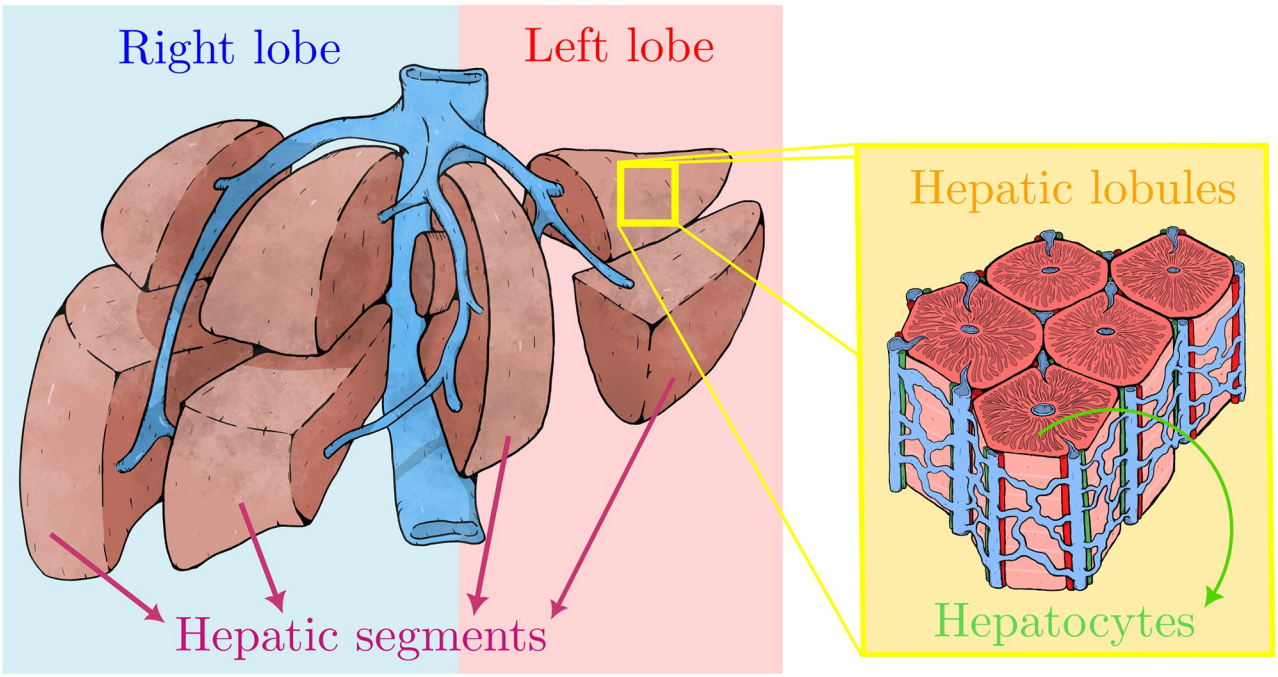

Fig 1. Schematic representation of the multi-scale liver architecture. The human liver is divided grossly into four parts or lobes. The four lobes are the right lobe, the left lobe, the caudate lobe, and the quadrate lobe. Seen from the front the liver is divided into two lobes: the right lobe and the left lobe. It is further divided in eight functionally independent segments based in the the Couinaud classification of liver anatomy. At the microscopic (histological) scale, the liver is organized in repetitive functional units called liver lobules, which take the shape of polygonal prisms (typically hexagonal in cross section). Each lobule is mainly constituted by hepatocytes and it is centered on a branch of the hepatic vein called the central vein which is interconnected with the interlobular portal triads: the hepatic artery (red), the portal vein (blue), bile duct (green).

https://doi.org/10.1371/journal.pcbi.1010920.g001

liver donation [69]. The multilobular structure of the liver not only allows the surgical resection of a lobe of choice to achieve different degrees by partial hepatectomy but also the resection of lobes does not induce damage to the remaining tissue. The extent of resection is determined by the size and location of the focal lesion and the estimated function of the future liver remnant [70]. Prior to liver resection, surgeons have to assess the patient's individual risk for postoperative liver dysfunction. In case of malignant tumors, surgeons have to identify the surgical strategy best suited to allow radical oncological removal in order to avoid recurrence, without putting the patient at risk of postoperative liver failure due to excessive removal of liver mass [71–73].

The liver regenerates in a highly organized fashion after surgery [68]. The human body responds to partial hepatectomy not by regenerating lost segments but by inducing hyperplasia in the remnant liver [36, 74, 75]. The anatomical structures of a liver that has undergone partial hepatectomy are therefore distinctly different from those of the original liver. The process of restoration of liver volume is initiated by the replication of various types of intrahepatic cells, followed by an increase in cell size. Nonparenchymal cells replicate in a delayed fashion. After replication has been completed, growth consisting of an increase in cell size occurs over several additional days. The initiation and synchronization of replication in different types of hepatic cells depend on the extent of the resection, tissue damage, or both. Low-grade tissue damage (*e.g.*, toxic or ischemic injury) or a relatively small resection (removal of less than 30% of the liver) substantially reduces the replication rate, which also appears to be less synchronized than after a large resection (removal of 70% of the liver) [36, 68, 75].

Since all our results are compared with experimental data obtained from rodent models, it is important to mention that the process of hepatic regeneration in rodents and humans is similar, and the results obtained from rodents could be applicable to the human liver [76]. Moreover, the rat liver architecture can be compared with the human liver segmentation defined by Couinaud [77].

2.2 Computational model

Our model is implemented resorting to an object oriented programming model, and to that aim we have used C++11 language. Simulation CPU time depends on model parameters such as domain (lattice) size, cell number and simulation length (in time); a typical simulation run takes approximately 6 h on a single core of an Intel i7–10510U CPU. Model visualization is performed with Ovito [78], Paraview [79] and Matplotlib [80].

In order to reduce the computational burden of the simulations, an abstraction process was necessary to go from the biological to the computational model. First, we disregard the explicit liver geometry, instead we have chosen a reduced spherical model. This simplification is possible because, as it was mentioned in section 2.1, after a PH the liver does not regenerate the lost segments, *i.e.* does not recover the original shape. Instead it just recovers its original volume by hyperplasia of the remaining lobes. Subsequently, we rather focus our attention on the liver parenchyma instead of liver lobes. In our computational model, hepatic lobules are hexagonal prisms delimited by an imaginary perimeter of interlobular portal triads. The central vein that carries the blood out from the liver as well as the liver sinusoids are not explicitly modeled as the portal triads are. We rather model this behavior by tuning the effective oxygen difussion and decay constants. A discussion on the implications of these simplifications on the results will be presented in section 4.

In the following subsections we will describe the methods implemented to model diffusion and cellular mechanics, as well as the mathematical models to predict tissue growth kinetics. For further details, we refer the reader to the supplementary material S1 Text. A schematic representation of the inner workings of our model is depicted in Fig 2. The key elements of the model are described in what follows.

2.2.1 Diffusion solver. We model the diffusion of chemical substrates in the tumor microenvironment as a vector of reaction-diffusion partial differential equations for a vector of chemical substrates, ρ. It is discretized over a Cartesian mesh for computational convenience, in such a way that each voxel (volumetric pixel) stores a vector of chemical substrates. Each substrate diffuses and decays, and can be secreted or uptaken by individual cells at their specific positions.

We use a first order, implicit (and stable) operator splitting, allowing us to create separate, optimized solvers for the diffusion-decay, cell-based source/sinks [81]. The diffusion-decay terms are solved using the finite volume method [82], further accelerated by an additional first-order spatial splitting in the x–, y– and z–directions via the locally one-dimensional method (LOD) [81, 83]. For each dimension, we solve the resulting tridiagonal linear systems with the Thomas algorithm [84].

We also implement the so-called Dirichlet nodes, so that substrate values at any voxel within the simulation domain can be overwritten to turn the voxel into a continuous source of substrates. This is particularly useful to model the effect of blood vessels, or when applying Dirichlet boundary conditions.

For computational efficiency we use thread parallelization to relevant loops, e.g. in many instances of the Thomas solver when solving x–diffusion across multiple strips of the solution domain. This methods were already implemented and successfully tested by Ghaffarizade et al.

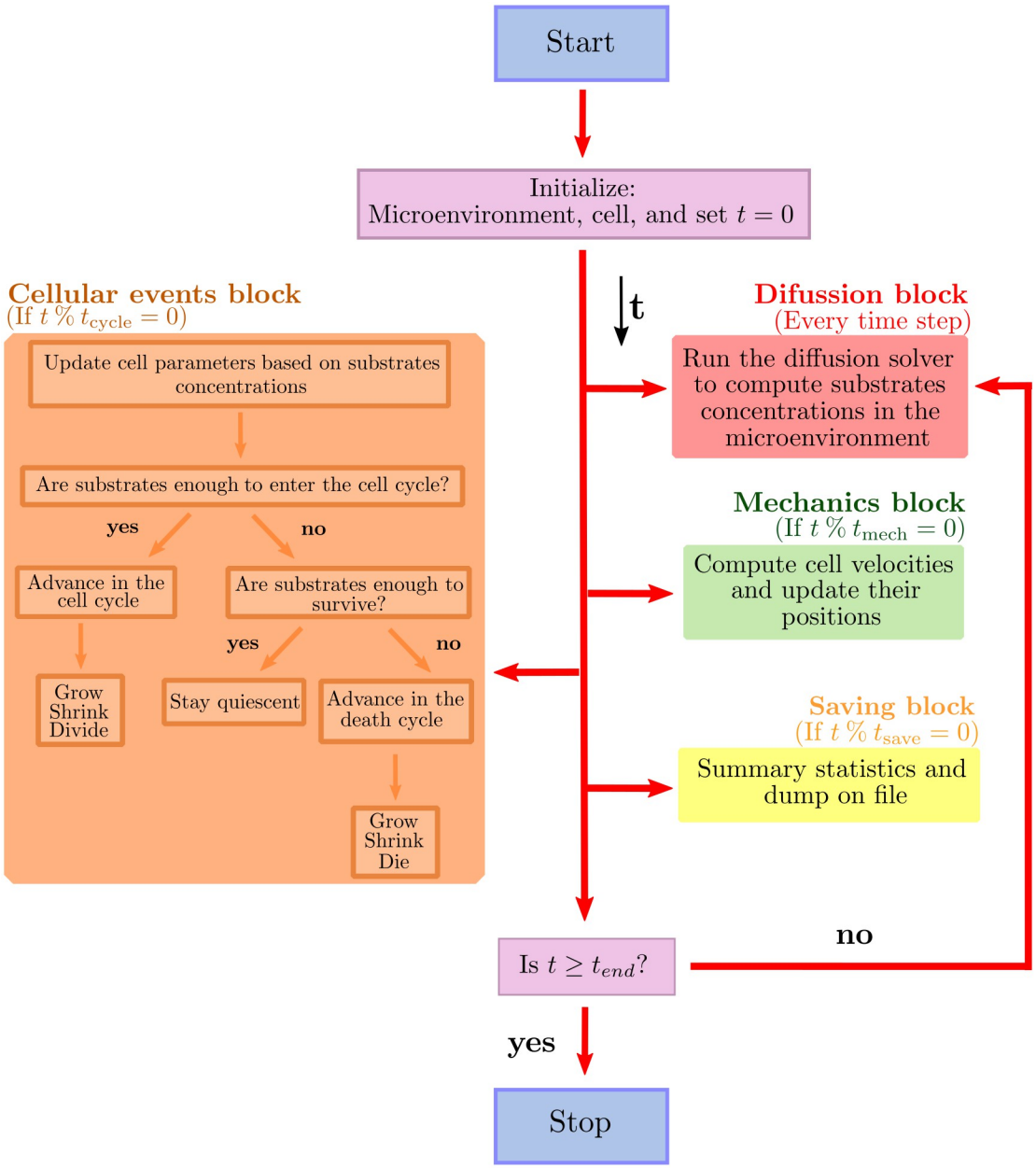

Fig 2. Main loop flow diagram. Blue box represents the start of the program. Red box represent the diffusion processes. Green box and orange box describe the cell mechanics and cycling processes respectively. Finally, yellow boxes represent the data saving process. After initializing the microenvironment, the cells, and the current simulation time $t = 0$, our model tracks (internally) t_{mech} (the next time at which cell mechanics methods are run), t_{cycle} (the next time at which cell processes are run), and t_{save} (the simulation data output time), with output frequency Δt_{save}. % represents the modulo operation.

https://doi.org/10.1371/journal.pcbi.1010920.g002

[85], therefore, we have validated the numerical accuracy of our solver by comparing our results with those found in Reference [85]. For further details, please refer to the supplementary material S1 Text.

2.2.2 Cell agents. Since we are implementing an agent-based model programmed in the context of an object oriented approach, each cell is an agent implemented as a software object that acts independently. Like most classes in software it has *attributes*, *i.e.* its own internal

variables that each specific agent is allowed to manipulate on its own. It also has *methods*, which are functions that act upon the attributes. In the context of cell biology, relevant attributes might be: position, size, cell state regarding the cell cycle, etc. The cell cycle is an object with the aforementioned attributes. The cell class have methods that represent cellular processes such as, death, growth and volume change, and are coordinated by the cell cycle object.

One of the main features of our model is that cells are *off-lattice*. Consequently, they are not confined to a particular lattice or spatial arrangement, they move in a continuous fashion through all space positions, and therefore underlying possible artifacts associated with the chosen lattice structure and spacing are removed.

Based on previous cell-based models [33, 86, 87], we have modeled the cell behavior as follows:

Cell cycle: We model the cell cycle as a directed graph, in which the nodes represent the phases and the edges the transition rates between them. These transition rates can take stochastic or constant values. Moreover, any of the cell cycle time scales can be adjusted at the beginning of the simulation to match different types of growth and they can also be adjusted at any time on an individual cell in order to reflect its microenvironment influences.

Our model allows to implement different types of cell cycles based on different parameters. Following Miyaoka and coworkers [44, 45], we can base our cell cycle on a tracking of the expression of protein Ki-67, involved in cell proliferation. This tracking is performed thanks to a nuclear stain of Ki-67. We note in passing that Ki-67 protein expresses in the *S*, *G*2, and *M* phases [88], and to a lesser extent in the *G*1 phase [89]. It is seen in post-mitotic daughter cells [90], but it is not produced in these cells [88]. Instead, any remaining Ki-67 protein in post-mitotic cells is degraded quickly, with a half-life of 60 − 90 minutes [88]. We can base our cell cycle by setting the phase "Ki-67+ pre-mitotic" to be the combined duration of *S*, *G*2, and *M* phases, which are relatively fixed compared to the duration of *G*0/*G*1 [91, 92]. We can set the second phase "Ki-67+ post-mitotic" at the *G*1/*G*0 phase, to be on the order of two Ki-67 half-lives. Then, the remaining *G*1/*G*0 phase will be the "Ki-67-" phase. For further details, please refer to the supplementary material S1 Text.

Finally, since at cell scale death is not an instantaneous event but a process, we model death cycles such as Necrosis and Apoptosis as we did with cell cycles, by using directed graphs, death is part of the cell cycle after all. The entry to the death cycles depends on the resources, for example oxygen, drugs, therapies, etc.

Cell volume: To model cell volume variation, each cell tracks V (total volume), V_F (total fluid volume), V_S (total solid volume), V_{NS} (nuclear solid volume), V_{CS} (cytoplasmic solid volume), V_N (total nuclear volume), and V_C (total cytoplasmic volume). Key parameters include nuclear solid, cytoplasmic solid, and fluid rate change parameters (r_N, r_C, and r_F), the cell's "target" fluid fraction f_F, target solid volume V^*_{NS}, and target cytoplasmic to nuclear volume ratio f_{CN}. For each cell, these volumes are modeled with a system of ordinary differential equations that allow cells to grow or shrink towards a target volume. These parameters are updated as the cell progresses through its current cycle or death cycle.

Cell mechanics: In our model, as in [33], we use the piecewise polynomial force which is constructed as the sum of a positive adhesive and a negative repulsive polynomial force contributions. It is important to note that repulsive forces are really an elastic resistance to deformation. To compute these forces we use adhesive and repulsive interaction potentials functions.

We assume that three types of forces act upon each cell. First we have a drag force, which represents dissipative drag-like forces such as fluid drag and cell-extra cellular matrix adhesion. We then have neighboring cell mechanical forces. In the simplest case these involve repulsive forces due to limited cell compressibility, but they usually also include cell-cell adhesion. We use interaction potentials that depend upon each cell's size, maximum adhesion

distance, adhesion and repulsion parameters and distance to other cells. Finally, the third force acting on the cells is the cell-basement membrane interaction.

Since the cell microenvironment has a very low Reynolds number (the Reynolds number describes the ratio of inertial to viscous forces) [93], inertial effects such as acceleration are neglected. This is commonly known as the inertialess assumption, and implies that forces equilibrate at relatively fast time scales in contrast to the processes involved in cell cycling, death cycling, and volume variation.

We finally use the Adams-Bashforth method [94] to solve the mechanics equation to enhance computational efficiency.

We refer the reader to the supplementary material S1 Text for further details on the implementation of the piecewise polynomial force model.

Cell secretion and uptake: This is one of the most important data structures of the cell because it links the cell with its microenvironment. We solve a vector of partial differential equations, which reduce to the addition of a cellular secretion/uptake term to the diffusion equation described in section 2.2.1.

This is very important since most of the cellular processes depend on the substrates that diffuse in the microenvironment. For example, it is well accepted that after a partial hepatectomy, the liver undergoes to cytokine- and growth factor- mediated regeneration processes [95]. However, most of the mechanisms of initiating and promoting regenerative responses as well as the termination of liver regeneration remain unknown [44, 45]. In this work cellular proliferation is assumed to be controlled by a growth factor that diffuses through the microenvironment. This growth factor is only considered as an abstract parameter which encompasses all the underlying molecular mechanisms involved in the liver regeneration process. The cell cycle entry rate is proportional to this factor in the following way:

$$r = \frac{1}{t_{K^-}} \max\left\{\left(\frac{GF - GF_{\text{prol}}}{GF^* - GF_{\text{prol}}}\right), 0\right\} \tag{1}$$

where t_{K^-} is the mean time each cell spends in the non-proliferative phase (see section 2.2.2), which can be experimentally monitored using the Ki-67 cellular marker. GF is the current growth factor concentration value in the cell's voxel, GF_{prol} is the proliferation threshold, *i.e.* the growth factor value below which the proliferation ceases and GF^* is the proliferation saturation value, above which the proliferation rate is maximized. Therefore, based on the growth factor concentration, the hepatocyte will enter either the hypertrophy phase or the proliferation phase. A similar approach can be done based on the oxygen concentration, however, instead of influence on the decision about whether or not to proliferate, oxygen will accelerate the phase entry. Please refer to the supplementary material S1 Text for further information about how cell cycles and transition rates will be modified based on chemical substrates concentrations.

2.3 Growth estimations

To complement our model in the prediction of tumor growth and/or tissue regeneration we use a mathematical model known as the *Gompertz model* [96–99]. This model assumes initial exponential growth, but as the tumor grows the volume-doubling time increases due to lack of nutrients and subsequent cell death, by which the growth rate shifts towards linear regime, finally reaching a plateau [96]. This is given by:

$$V(t) = K \ \exp\left[\log\left(\frac{V_0}{K}\right)\exp(-\alpha t)\right] \tag{2}$$

where the parameter K is the carrying capacity of the tissue, which is the highest possible volume, V_0 is the initial volume of the tissue and α is the specific growth rate [100, 101] which is defined by

$$\alpha = \frac{\log\left(\frac{V_2}{V_1}\right)}{t_2 - t_1}. \tag{3}$$

Here V_1 and V_2 are tumor volumes at the measure times t_1 and t_2 respectively. This parameter α determines how fast the tumor reaches the carrying capacity K and its measured in (%/days).

3 Results

We first attempted to define a baseline scenario of the liver physiology. As it was mentioned before, we focus our attention in the liver parenchyma which, in our model, is made up of hepatic lobules which are hexagonal prisms delimited by an imaginary perimeter of interlobular portal triads. We idealized this dynamic vasculature architecture (Fig 3a) by using the Dirichlet nodes as shown in Fig 3b and 3c, and defining the distance between triads on micrograph analysis [66]. Fig 3b shows a transversal cut of our simulated liver in which we can observe the hepatic lobules architecture. Blue dotted lines were drawn just as a guide to the eye. Pink spheres represent the hepatocytes and the white squares represent the portal triads that oxygenate the tissue. Fig 3c shows the heat map of the oxygen diffusion in the liver micoenvironment. The oxygen diffuses from the portal triads (Dirichlet nodes), there is no diffusion from the boundaries of the simulation box.

The grid we used to simulate liver regeneration is 1 mm^3 in total size, orders of magnitude smaller than an actual liver. While the model does not place limitations on the liver size, the implementation is obviously constrained by the size of the computer memory. However, this limitation can be to some extent circumvented by considering the sample region as representative of a significant sub-region of the liver. Obviously size effects must be investigated in further detail to the extent that new algorithmic and hardware improvements become available (e.g. by exploiting massively parallel CUDA [102] cores and/or Tensor cores in new GPU/TPU architectures).

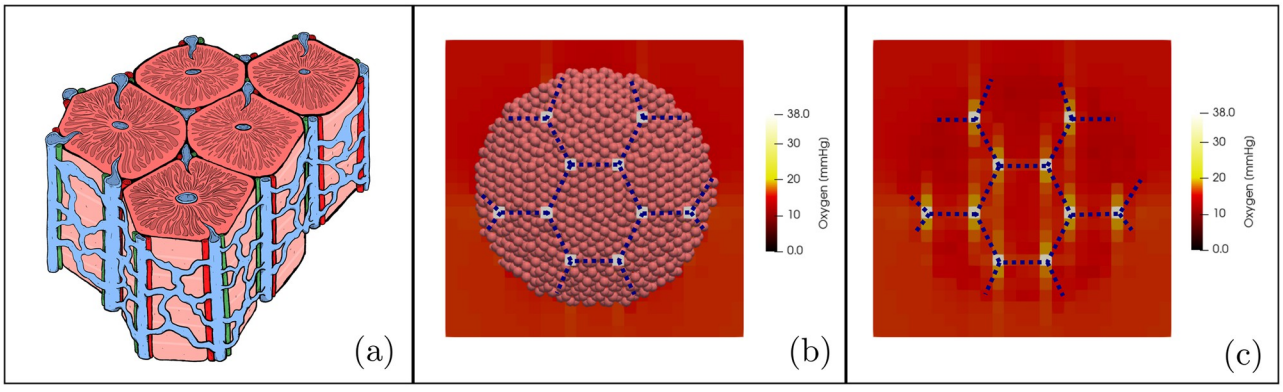

Fig 3. Liver blood vessels architecture. (a) Schematic representation of the hepatic lobules. They consist of plates of hepatocytes, and sinusoids radiating from a central vein interconnected with the interlobular portal triads: the hepatic artery (red), the portal vein (blue), and the common bile duct (green). **(b)** computational model of the liver parenchyma in which we can observe the blood vessel architecture. **(c)** Heat map of the oxygen diffusion in the liver microenvironment. Blue dotted lines were drawn just as a guide to the eye.

https://doi.org/10.1371/journal.pcbi.1010920.g003

1.1 Input parameters

Parameter	Description	Units
Microenvironment Parameters		
$\Omega_x, \Omega_y, \Omega_z$	Domain size	μm
$\Delta x, \Delta y, \Delta z$	Microenvironment voxel size	μm
D	Substrates diffusion coefficients	μm^2/min
λ	Substrates decay rates	min^{-1}
BC	Set the boundary conditions	dimensionless
ρ_{BC}	BC substrates concentration	multiple
Cell Parameters		
V	Total cell volume	μm^3
V_N	Total nuclear volume	μm^3
f_{CN}	Target cytoplasmic:nuclear volume ratio	dimensionless
f_F	Target fluid fraction	dimensionless
ρ^*	Substrates saturation value	multiple
ρ_{thres}	Substrates threshold value	multiple
S	Substrates release rate	min^{-1}
U	Substrates uptake rate	min^{-1}
Cell Cycle Parameters		
T_{G1}	Duration of G_1 phase	hs
T_S	Duration of S phase	hs
T_{G2}	Duration of G_2 phase	hs
T_M	Duration of M phase	hs
div_{prob}	% of cells allowed to divide	dimensionless
Cell Mechanics Parameters		
n_x, n_y, n_z	Mechanics discretization voxel size	μm
R_A	Maximum cell adhesion distance	μm
$C_{ccr/a}$	Cell-cell “repulsive”/adhesion force constant	μm/min
$C_{cmr/a}$	Cell-membrane “repulsive”/adhesion force constant	μm/min
p	Division polarization	dimensionless

Table 1: Input parameters.

Parameter	Description	Units
Time Parameters		
T_{Tot}	Total simulation time	min
t_{save}	Saving time	min
Δt_{cycle}	Cell processes time step	min
Δt_{mech}	Cell mechanics time step	min
Δt_{diff}	Diffusion time step	min
t_v	Update voxel lists of particles time	min

Table 2: Time input parameters.

1.2 Output parameters

Every t_{save} the program saves the following information:

Parameter	Description	Units
Microenvironment Parameters		
Ω_m	Cell's microenvironment voxel	dimensionless
ρ_{O_2}	O_2 concentration in cell's voxel	mmHg
ρ_{Imm}	Immunostimulatory factor concentration in cell's voxel	dimensionless
ρ_{GF}	Growth factor concentration in cell's voxel	dimensionless
Cell Parameters		
ID	Cell's ID	dimensionless
Ω_{mech}	Cell's mechanical voxel	dimensionless
x, y, z	Cell's center position	dimensionless
r	Cell's radii	μm
op	Cell's oncoprotein expression	dimensionless
Type	Cell type, *i.e* cancer, hepatocyte, etc	dimensionless
Cycle	Cell or death cycle	dimensionless
Progenitor	Cell progenitor's ID	dimensionless

Table 3: Output parameters.

2 Biochemical microenvironment

Tissues are filled with various chemical compounds, including signaling and other factors that regulate how cells move, grow, and die, depending on the concentration and/or gradient of any and all of these compounds. In order for cells to survive and grow, they need to obtain oxygen and other nutrients released from blood vessels. In general, they need the interaction with the

4 Parameters for the main examples

4.1 General

Parameter	Value	Units	Reference
Microenvironment Parameters			
$\Omega_x \times \Omega_y \times \Omega_z$	$1000 \times 1000 \times 1000$	μm	-
$\Delta x \times \Delta y \times \Delta z$	$20 \times 20 \times 20$	μm	-
D_{O_2}	10^5	μm^2/min	[77]
λ_{O_2}	0.1	min^{-1}	[37]
D_{GF}	10^6	μm^2/min	-
λ_{GF}	0.5	min^{-1}	-
BC	No flux at the boundaries	-	-
$\rho_{vessels,O_2}$	38	mmHg	[78]
Cell Mechanics Parameters			
n_x, n_y, n_z	$30 \times 30 \times 30$	μm	-
R_A	$1.25R_{cell}$	μm	[40]
C_{ccr}	10.0ν	μm/min	[79]
C_{cmr}	C_{ccr}	μm/min	-
p	0	dimensionless	-

Table 4: Numerical values of the input parameters used in all the examples.

Time Parameters			
Parameter	Value	Units	Reference
t_{Tot}	43200	min	-
t_{save}	1440	min	-
Δt_{cycle}	6	min	[36]
Δt_{mech}	0.1	min	[36]
Δt_{diff}	0.01	min	[36]
t_v	$20\Delta t_{mech}$	min	-

Table 5: Times used in all the examples.

4.2 Liver regeneration

Parameter	Value	Units	Reference
Cell Parameters			
V	8000	μm^3	[80]
V_N	268	μm^3	[81]
O_2^*	38	mmHg	-
$O_{2,prol}$	10	mmHg	-
GF_{prol}	0.25	dimensionless	-
S_{O_2}	0	min^{-1}	-
U_{O_2}	10	min^{-1}	-
Cell Cycle Parameters			
t_{G1}	21.6	hs	[82]
t_S	7.0	hs	[82]
t_{G2}	3.4	hs	[82]
t_M	1.6	hs	[82]
n_{div}	1	dimensionless	[16]
div_{prob}	0.7	dimensionless	[16]

Table 6: Numerical values used for liver regeneration

4.3 Tumor growth

Parameter	Value	Units	Reference
Cell Parameters			
V	8000	μm^3	[80]
V_N	268	μm^3	[81]
O_2^*	38	mmHg	-
$O_{2,prol}$	10	mmHg	-
S_{O_2}	0	min^{-1}	-
U_{O_2}	10	min^{-1}	-
Cell Cycle Parameters			
t_{G1}	20.4	hs	[82]
t_S	13.6	hs	[82]
t_{G2}	3.0	hs	[82]
t_M	1.6	hs	[82]
n_{div}	∞	dimensionless	-

Table 7: Numerical values used for Hepatocellular carcinoma recurrence